Available online at www.sciencedirect.com
SCIENCE DIRECT®
International Journal of Heat and Mass Transfer 49 (2006) 269–280
International Journal of HEAT and MASS TRANSFER
www.elsevier.com/locate/ijhmt

Thermal stability of a nonuniformly heat generating annular fluid layer

S. Saravanan, P. Kandaswamy *

UGC-DRS Center for Fluid Dynamics, Department of Mathematics, Bharathiar University, Coimbatore 641 046, Tamil Nadu, India

Received 21 May 2004; received in revised form 1 January 2005
Available online 1 December 2005

Abstract

The thermal stability of two dimensional parallel convective motion in a fluid confined between two vertical cylinders is studied. The convective motion is induced by nonuniformly distributed heat sources in the fluid layer. A spectral collocation method is employed to solve the axisymmetric perturbed equations arising in the linear stability analysis. The stability boundary depends on the source distribution parameter, source strength parameter, Prandtl number and radius ratio. In general the flow remains least stable when the source distribution parameter is maximum in the middle of the two bounding cylinders. Thermal buoyancy mode of instability is introduced by the source distribution parameter for lower values of the radius ratio.

1. Introduction

In the presence of adverse temperature distribution, potentially unstable situations arise in which denser fluid lies above less dense fluid. Such a situation may happen by heating a quiescent fluid either from below or within. The study of stability of fluid layers with internal heat generation has received considerable attention owing to the significance of convection in earth's core leading to volcanic eruptions and nuclear reactor design safety. Thermal convection in a fluid with internal heat sources is important in the theory of thermal ignition where heat sources within the fluid are driven by an exothermic chemical reaction. Here the thermal gradients originated by the chemical reaction is one of the driving force for the onset of convection and, in turn, responsible for the enhancement of heat transfer rate.

Vasquez [1], Garbey et al. [2] and Zeldovich et al. [3] have studied convective chemical fronts with a detailed list of references. The effect of nonlinear temperature profile resulting from uniform internal heat generation in a horizontal fluid layer was studied by Sparrow et al. [4]. Acharya and Goldstein [5], May [6] and Churbanov et al. [7] presented numerically the oscillating character of thermal convection in an enclosure with uniform heat sources. Suo-Antilla and Catton [8] and Kulacki and Goldstein [9] investigated the stability criteria for various hydrodynamic and thermal boundary conditions.

The study of heat generation within a fluid layer because of chemical reaction and absorption of incident radiation as in a Laser Doppler Velocimeter requires a thorough knowledge of nonuniform volumetric energy sources. Yucel and Bayazitoglu [10], Shaaban and

* Corresponding author. Tel.: +91 422 2422222; fax: +91 422 2422387.
E-mail addresses: sshravan@lycos.com (S. Saravanan), pgkswamy@yahoo.co.in (P. Kandaswamy).

0017-9310/$ - see front matter © 2005 Elsevier Ltd. All rights reserved.
doi:10.1016/j.ijheatmasstransfer.2005.06.033

Nomenclature

b	$100\frac{\beta-r_1}{r_2-r_1}$, source distribution parameter
c	wave speed
c_p	specific heat capacity
g	acceleration due to gravity
Gr	Grashof number
h	half annulus width
k	wave number
$\hat{k}$	unit vector in the z direction
n	number of collocation points
N	normalization factor such that $\int_{r_1}^{r_2}\frac{Q(r)}{Q_0}\,dr = C'$
p	pressure
P	performance index
Q	volume density of internal heat sources
Q_0	constant
r	radial coordinate
r_1	$2R/(1-R)$, dimensionless radius of inner cylinder
r_2	$2/(1-R)$, dimensionless radius of outer cylinder
R	R_1/R_2, radius ratio
R_1	radius of inner cylinder
R_2	radius of outer cylinder
M	$1/\max[(r_1-\beta)^2, (r_2-\beta)^2]$
t	nondimensional time
T	nondimensional temperature
$\bar{v}$	nondimensional velocity vector
z	axial coordinate

Greek symbols

α	source strength parameter
β	source distribution parameter
ν	kinematic viscosity
κ	thermal diffusivity
λ	complex eigenvalue
ϕ	quantity introduced in Eq. (19)
θ	quantity introduced in Eq. (19)
ρ	density
Φ	dimensionless stream function
∇	gradient

Superscript

*	dimensional quantity

Subscripts

c	critical value
0	basic state

Ozisik [11] and Kolyshkin and Vaillancourt [12] have applied linear theory stability criteria and studied thermal stability with various values of the nonuniformity source parameter. Fluid models with nonuniform heat generation are also used for the analysis of photochemical reactors and the theory of thermal ignition (see [13,14]).

Curvature effect should be taken into account in problems dealing with fluid layers as it plays a significant role in natural and manmade phenomena like convection between earth's tectonic plates and convection in molten heat generating corium layer surrounding the core in a Pressurized Water Reactor [7]. A survey of the literature indicates that in the studies dealing with stability of convection driven by nonuniform heat sources in fluid layers, only the effect of different source strengths have been investigated. But in reality, chemical reactions occurring can also change the source distribution within the fluid medium. In batteries with flowing electrolytes which are operating at high rates, the species concentration distribution could be highly nonuniform and result in spatially nonuniform exothermic reaction rates (see [15]). Most of the batteries are cylindrical in nature with centrosymmetric ingredients. This makes the exothermic reaction rate to change in the radial direction alone. Spatially nonuniform heating due to absorption of incident radiation has been reported by Davis and Zheng [16]. In this photochemical reaction the heat source gets concentrated near the surface which is exposed to laser light. Thus circumferential application of the laser light to a body of photosensitive fluid makes the heat source distribution as a function of radial direction alone. Motivated by the above factors, in this paper we study the thermal stability of a vertical annular fluid layer with nonuniformly distributed heat sources.

2. Mathematical analysis

Let us consider an infinitely long vertical annular channel confined between two concentric cylinders of radii R_1 and R_2 ($R_1 < R_2$) enclosing a viscous incompressible fluid. The temperatures of both cylinder walls are kept constant and equal. We choose a cylindrical polar coordinate system, where the z-axis is directed opposite to gravity **g** (Fig. 1). The origin of the coordinate system is located on the cylinders' axis. The fluid is heated with a nonuniform volumetric energy source Q. All the physical characteristics are taken as constant, except the density which varies linearly with temperature in the buoyancy term (Boussinesq approximation).

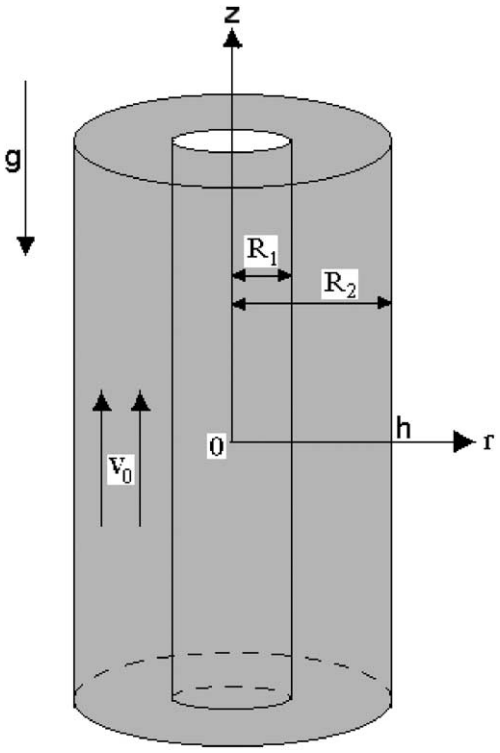

Fig. 1. A diametral cross-section of the physical configuration.

The equations governing the motion of a viscous incompressible fluid in the above configuration under the Boussinesq approximation are

$$\frac{\partial \bar{v}^*}{\partial t^*} + (\bar{v}^* \cdot \nabla^*)\bar{v}^* = -\frac{1}{\rho}\nabla^* p^* + \nu(\nabla^*)^2 \bar{v}^* + g\beta T\hat{k} \tag{1}$$

$$\frac{\partial T^*}{\partial t^*} + (\bar{v}^* \cdot \nabla^*)T^* = \kappa(\nabla^*)^2 T + \frac{Q}{\rho c_p} \tag{2}$$

$$\operatorname{div} \bar{v}^* = 0 \tag{3}$$

The thermal convection of the fluid is produced by internal heat sources of volume density

$$Q(r) = Q_0 e^{\alpha N[1-M(r-\beta)^2]} \tag{4}$$

where α is the source strength parameter, β the source distribution parameter such that $r_1 \leqslant \beta \leqslant r_2$, r_1 and r_2 being the dimensionless radii of the cylinders, N the normalization factor chosen such that $\int_{r_1}^{r_2} \frac{Q(r)}{Q_0}\,dr = \frac{C}{Q_0} = C'$, where C and C' are constants for varying β and $M = 1/\max[(r_1-\beta)^2, (r_2-\beta)^2]$. When $\beta = r_1$ and r_2, Q is nearer to the inner and outer cylinders respectively. The distribution (4) may be caused by radially varying heat sources in the annular region, uniform in the azimuthal and axial directions. An exponential distribution similar to (4) may result from a zeroth order reaction [14] or absorption of incident radiation [10,13].

We define $h = (R_2 - R_1)/2$, $R = R_1/R_2$, $r_1 = 2R/(1-R)$, $r_2 = 2/(1-R)$ and introduce the nondimensional variables $r = r^*/h$, $z = z^*/h$, $t = t^*/(h^2/\nu)$, $\bar{v} = \bar{v}^*/(g\beta q h^4/2\nu)$, $p = p^*/(\rho g\beta h^3/2)$, $T = T^*/(qh^2/2)$. Let $Gr = g\beta q h^5/2\nu^2$ be the Grashof number, $Pr = \nu/\kappa$ the Prandtl number and $q = Q/(\rho c_p \kappa)$. In dimensionless variables, Eqs. (1)–(3) become

$$\frac{\partial \bar{v}}{\partial t} + Gr(\bar{v}\cdot\nabla)\bar{v} = -\nabla p + \nabla^2 \bar{v} + T\hat{k} \tag{5}$$

$$\frac{\partial T}{\partial t} + Gr(\bar{v}\cdot\nabla)T = \frac{1}{Pr}\nabla^2 T + \frac{2}{Pr} e^{\alpha N[1-M(r-\beta)^2]} \tag{6}$$

$$\operatorname{div} \bar{v} = 0 \tag{7}$$

where $\bar{v}$, T and p are respectively, the velocity of the fluid, temperature and pressure. We seek a steady parallel solution for Eqs. (5)–(7) of the following type:

$$\bar{v} = [0, 0, v_0(r)], \quad T = T_0(r), \quad p = p_0(z) \tag{8}$$

The flow (8), may be realized in the middle portion of a sufficiently long vertical layer of fluid where the end effects are negligible. Substituting Eq. (8) into Eqs. (5)–(7) leads to the system

$$\frac{d^2 v_0}{dr^2} + \frac{1}{r}\frac{dv_0}{dr} + T_0 = D \tag{9}$$

$$\frac{d^2 T_0}{dr^2} + \frac{1}{r}\frac{dT_0}{dr} = -2e^{\alpha N[1-M(r-\beta)^2]} \tag{10}$$

where D is the separation constant. The corresponding boundary conditions are

$$v_0(r_i) = 0, \quad T_0(r_i) = 0, \qquad i = 1, 2 \tag{11}$$

The solution at the basic state is given by

$$T_0(r) = -\frac{a_0}{2}r^2 - \frac{2a_1}{9}r^3 - \frac{a_2}{8}r^4 - \frac{2a_3}{25}r^5 - \frac{a_4}{18}r^6 + A\log r + B \tag{12}$$

$$v_0(r) = \frac{D + A - B}{4}r^2 + \frac{a_0}{32}r^4 + \frac{2a_1}{225}r^5 + \frac{a_2}{288}r^6 + \frac{2a_3}{1225}r^7 + \frac{a_4}{1152}r^8 - \frac{A}{4}r^2\log r + E\log r + F \tag{13}$$

where

$$a_0 = 1 + \alpha N(1 - M\beta^2) + \frac{\alpha^2 N^2}{2}(1 - M\beta^2)^2$$

$$a_1 = 2\alpha N M\beta + 2\alpha^2 N^2 M\beta(1 - M\beta^2)$$

$$a_2 = -\alpha N M + 2\alpha^2 N^2 M^2\beta^2 - \alpha^2 N^2 M(1 - M\beta^2)$$

$$a_3 = -2\alpha^2 N^2 M^2 \beta$$

$$a_4 = \frac{\alpha^2 N^2 M^2}{2}$$

$$A = -\frac{1}{\log R}\left[\frac{a_0}{2}(r_2^2 - r_1^2) + \frac{2a_1}{9}(r_2^3 - r_1^3) + \frac{a_2}{8}(r_2^4 - r_1^4) + \frac{2a_3}{25}(r_2^5 - r_1^5) + \frac{a_4}{18}(r_2^6 - r_1^6)\right]$$

$$B=\frac{a_0}{2}r_2^2+\frac{2a_1}{9}r_2^3+\frac{a_2}{8}r_2^4+\frac{2a_3}{25}r_2^6+\frac{a_4}{18}r_2^8-A\log r_1,$$
$$E=\frac{D+A-B}{4\log R}(r_2^2-r_1^2)+\frac{a_0}{32\log R}(r_2^4-r_1^4)+\frac{2a_1}{225\log R}(r_2^5-r_1^5)$$
$$+\frac{a_2}{288\log R}(r_2^6-r_1^6)+\frac{2a_3}{1225\log R}(r_2^7-r_1^7)$$
$$+\frac{a_4}{1152\log R}(r_2^8-r_1^8)-\frac{A}{4\log R}(r_2^2\log r_2-r_1^2\log r_1),$$
$$F=-\frac{D+A-B}{4}r_1^2-32a_0r_1^4-\frac{2a_1}{225}r_1^5-\frac{a_2}{288}r_1^6$$
$$-\frac{2a_3}{1225}r_1^7-\frac{a_4}{1152}r_1^8+\frac{A}{4}r_1^2\log r_1-E\log r_1$$

We consider the case of a closed channel. This warrants the fluid flow through the cross-section of the channel to be zero and hence

$$\int_{r_1}^{r_2} rv_0(r)\,\mathrm{d}r=0 \tag{14}$$

The source distribution, basic temperature and velocity profiles for different values of b are shown in Figs. 2–4 in terms of the radial coordinate

$$x=r-\frac{1+R}{1-R}$$

We consider the stability of the basic state by the method of small perturbations. Let us consider the perturbed motion $\bar{v}_0+\bar{v}$, T_0+T, and p_0+p, where $\bar{v}$, T and p are small unsteady perturbations, $\bar{v}_0=v_0\hat{k}$. Let us assume that the perturbation in the velocity component v_θ is equal to zero and the other components v_r, v_z and perturbations of T and p do not depend on θ (so called axisymmetric perturbations). Then Eqs. (5)–(7) for the above perturbed state after linearization take the form

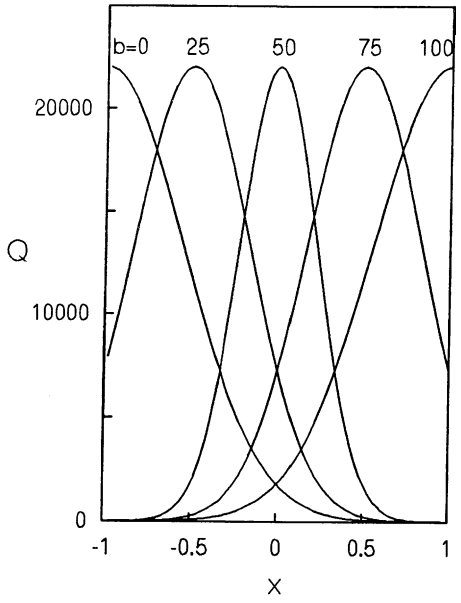

Fig. 2. Source distribution for different b when $R=0.4$, $\alpha=1$ and $C'=10$.

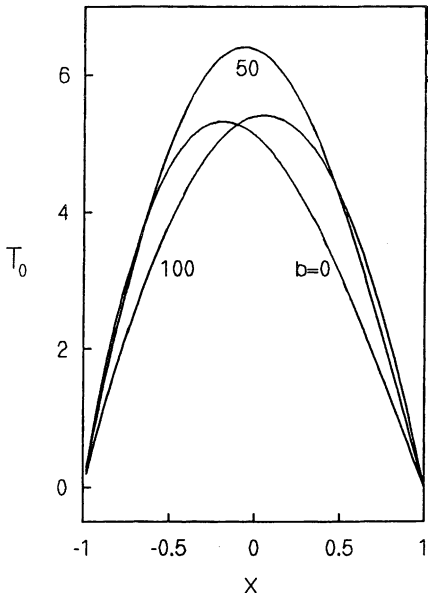

Fig. 3. Basic temperature profiles for different b when $R=0.4$, $\alpha=1$ and $C'=10$.

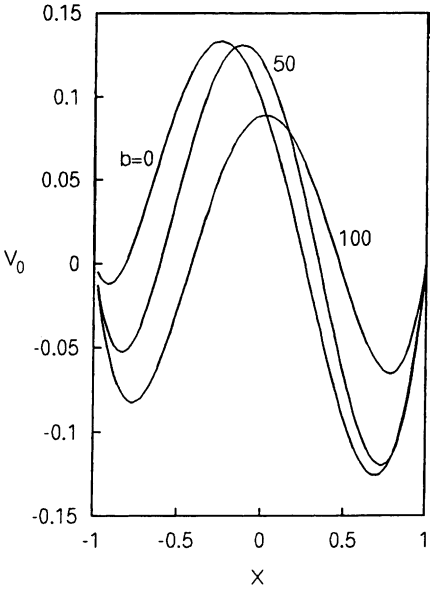

Fig. 4. Basic velocity profiles for different b when $R=0.4$, $\alpha=1$ and $C'=10$.

$$\frac{\partial\bar{v}}{\partial t}+Gr[(\bar{v}_0\cdot\nabla)\bar{v}+(\bar{v}\cdot\nabla)\bar{v}_0]=-\nabla p+\nabla^2\bar{v}+T\hat{k} \tag{15}$$
$$\frac{\partial T}{\partial t}+Gr(\bar{v}_0\cdot\nabla)T+(\bar{v}\cdot\nabla)T_0=\frac{1}{Pr}\nabla^2T \tag{16}$$
$$\mathrm{div}\,\bar{v}=0 \tag{17}$$

It is convenient to introduce the stream function $\Psi(r,z)$ as

$$v_r = -\frac{1}{r}\frac{\partial \Psi}{\partial z}, \quad v_z = -\frac{1}{r}\frac{\partial \Psi}{\partial x} \tag{18}$$

We set

$$\begin{aligned} \Psi(r,z,t) &= \phi(r)\exp(-\lambda t + \mathrm{i}kz) \\ T(r,z,t) &= \theta(r)\exp(-\lambda t + \mathrm{i}kz) \end{aligned} \tag{19}$$

where ϕ and θ are the amplitudes of the normal perturbations, k is the wave number and λ is a complex eigenvalue. Substituting Eq. (19) in Eqs. (15)–(17), we obtain the amplitude equations

$$\begin{aligned} L_1\phi = {} & 2k^2\phi^{(2)} - \frac{2k^2}{r}\phi^{(1)} - k^4\phi + \frac{k^2}{r^2}\phi \\ & + \mathrm{i}kGr\left(v_0\left(\phi^{(2)} - \frac{1}{r}\phi^{(1)} - k^2\phi\right) + \phi\left(\frac{v_0^{(1)}}{r} - v_0^{(2)}\right)\right) \\ & - r\theta^{(1)} - \lambda\left(\phi^{(2)} - \frac{1}{r}\phi^{(1)} - k^2\phi\right) \end{aligned} \tag{20}$$

$$L_2\theta = k^2\theta + \mathrm{i}kGrPr\left(v_0\theta - \frac{T_0^{(1)}}{r}\phi\right) - \lambda Pr\theta \tag{21}$$

where $L_1 = \left(r\frac{\mathrm{d}}{\mathrm{d}r}\left(\frac{1}{r}\frac{\mathrm{d}}{\mathrm{d}r}\right)\right)^2$, $L_2 = \frac{1}{r}\frac{\mathrm{d}}{\mathrm{d}r}\left(r\frac{\mathrm{d}}{\mathrm{d}r}\right)$.

The velocity and temperature perturbations vanish at the sidewalls and hence the boundary conditions are

$$\phi(r_i) = 0, \quad \phi^{(1)}(r_i) = 0, \quad \theta(r_i) = 0, \qquad i = 1,2 \tag{22}$$

Table 1
Critical Grashof number for different n ($Pr = 2$, $\alpha = 1$ and $C' = 10$)

n	$R = 0.4$, $b = 50$	$R = 0.4$, $b = 75$	$R = 0.7$, $b = 25$	$R = 0.7$, $b = 100$
3	376.73	465.84	453.02	498.00
7	63.12	76.21	77.20	80.60
10	65.99	80.18	79.25	87.27
12	63.86	78.34	78.99	87.11
13	63.14	77.24	78.61	87.08
14	62.71	76.48	78.48	87.06

We solve the boundary value problem using the spectral collocation method based on the roots of Chebyshev polynomials which was successfully implemented in our previous study [17]. The convergence of the numerical solution has been checked by varying the number of collocation points n. Table 1 shows the critical states for different combinations. We noticed that at $n = 14$ the 2% convergence criterion is met. Further increase in n considerably increases the cost. So we fixed n as 14 in our calculations. To ensure that the errors in eigenvalue computations are minimal for all the cases considered, we maintained the performance index (see [17]) below 0.8.

3. Results and discussion

Before discussing the stability properties of nonuniformly distributed heat source, it is interesting to compare our results, for different R with previous stability solutions. Table 2 presents a comparison between published critical conditions and the numerical values of the present investigation, at various Prandtl numbers. Gershuni et al. [18] used approximating polynomials of different degrees in their Galerkin method and so their results differ slightly. Still we observe a good agreement between the results at the same conditions which provides a further check on the numerical accuracy.

Computations were carried out for the radius ratios $R = 0.1$, 0.4 and 0.7. The interval $[r_1, r_2]$ was divided into 100 equal parts in such a way that $\beta = r_1 + b((r_2 - r_1)/100)$. Thus b may be treated as a source distribution parameter equivalent to β. We noticed that the shape of the marginal stability curve changes considerably if some of the parameters are changed. First of all we consider one such sample.

The effect of Pr on the stability characteristics is shown in Fig. 5 when $b = 25$ and $\alpha = 1$. For a low Pr approximation (i.e., $Pr = 0.01$) the marginal curve has a single minimum. The corresponding critical wave speed c_c is nearly zero (-0.02 more exactly). The wave speed is measured in the same units as the velocity of

Table 2
Comparison of the present results with others

R	Pr	Gr_c	k_c	c_c
0.9 (results of [18] are within braces)	1	733.43 (744)	1.36 (1.38)	−0.95 (−0.87)
	2	462.29 (470)	1.33 (1.35)	−1.14 (−1.04)
	3	353.03 (359)	1.33 (1.35)	−1.23 (−1.12)
	5	254.53 (259)	1.34 (1.35)	−1.33 (−1.21)
	10	167.82 (171)	1.36 (1.38)	−1.42 (−1.29)
	20	113.75 (115)	1.36 (1.40)	−1.51 (−1.36)
0.4 (results of [12] are within braces)	5	261.00 (262.4)	1.28 (1.33)	−1.11 (−1.18)
	20	114.73 (116.4)	1.30 (1.37)	−1.28 (−1.33)

the base flow and is normalized by the modulus of maximum velocity: $c = \mathrm{Im}(\lambda)/(kGrv_{0\max})$, where λ is a pure imaginary eigenvalue. Since the low Pr fluids are good conductors of heat, they immediately dissipate temperature disturbances before the disruption of buoyancy force causes instability. Hence the instability caused by the unstable velocity distribution by shearing action is referred to as shear (S) mode. On the other hand as Pr increases, the penetration depth of the temperature disturbances decreases and the buoyant force becomes more concentrated resulting in an instability. In the above figure, we see that Gr_c is considerably lowered with a corresponding shift towards the lower wave number region even for $Pr = 1$. Further increase in Pr results in the development of a nose-shaped piece in the marginal curve with a corresponding wave speed -1.11. This converts the marginal curve into two branches, having a local minimum in each one. Hence the nose-shaped part of the marginal curve represents the difference between the full stability problem and the Orr-Sommerfeld equation for the same velocity profiles. We observe that c_c shoots up with increasing Pr and exceeds even the mainstream velocity at $Pr = 5$. Thus the instability caused by fast moving thermal waves is referred to as thermal buoyant (TB) mode and is associated with a nose-shaped branch.

Let us see the deformation of the marginal curves for various values of the source distribution parameter b (Figs. 6 and 7). For this we fixed $R = 0.4$, $Pr = 2$ and $\alpha = 1$. When $b = 0$, the marginal curve of Gr is bimodal in nature as discussed above, with the lower and higher wave number minima corresponding to TB and S modes of instability. In these, TB mode is responsible for the onset of instability. This is expected when $b = 0$, because of the increased buoyancy force resulting from the steep density gradient for larger curvature. As b is increased upto 50, the nose-shaped part of the marginal curve starts disappearing resulting in a single minimum marginal curve. Thus S mode becomes critical at $b = 50$. We find that the basic flow is destabilized as b increases from 0 to 50. Further increase in b to 100 slightly stabilizes convection with S mode remaining critical. As b has the ability to change the density gradient considerably and hence the buoyancy force, TB modes are introduced in marginal curves. In general we find that perturbations corresponding to all wave numbers start moving downward. An increase in b results in an increase in c and hence c exceeds the base flow velocity. From the above discussion, we can expect somewhat symmetrical marginal curves for Gr as R takes larger values. Fig. 8 displays the situation for $R = 0.7$. Here we observe that Gr_c is symmetrical about $b = 50$.

The stability boundaries of convective motion in a wider gap ($R = 0.1$) on (b, Gr_c) plane are shown in Fig. 9 for various values of Pr. We notice that b produces two different effects. The flow at $b = 50$ is stabilized when b increases from 50 to 100 for smaller values of Pr ($Pr = 0.01$ and 0.5) and destabilized for higher values of Pr ($Pr = 3$ and 10). The basic state for all values of b are destabilized for increasing Pr.

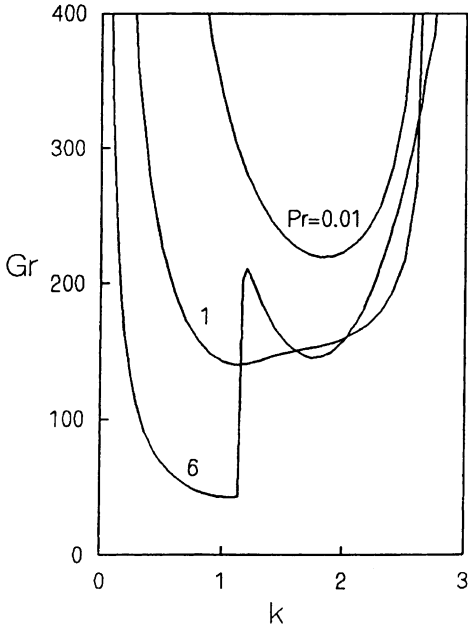

Fig. 5. Marginal stability curves for different Pr when $R = 0.4$, $\alpha = 1$, $b = 25$ and $C' = 10$.

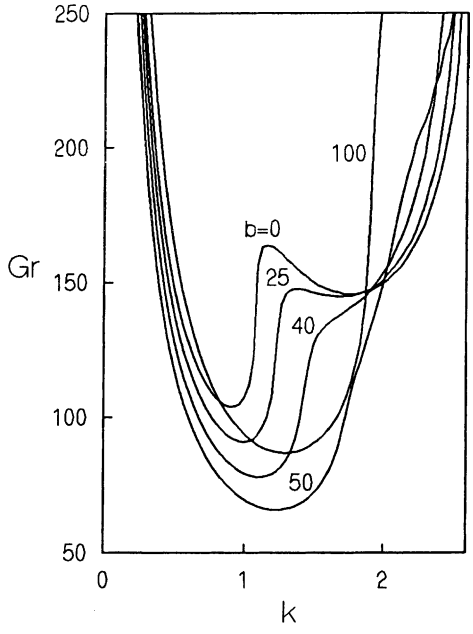

Fig. 6. Marginal stability curves for different b when $R = 0.4$, $\alpha = 1$, $C' = 10$ and $Pr = 2$.

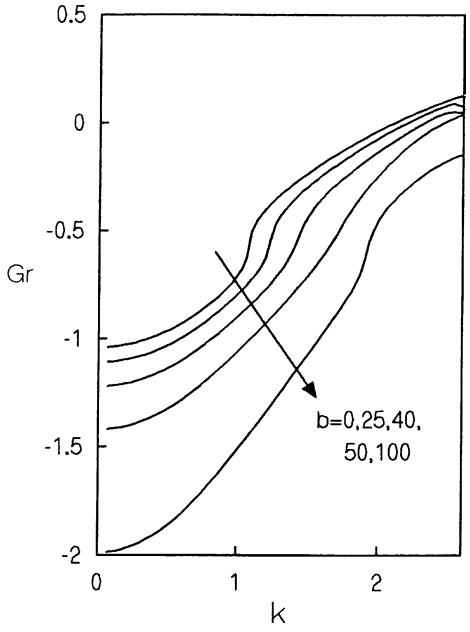

Fig. 7. Marginal wavespeeds for different b when $R = 0.4$, $\alpha = 1$, $C' = 10$ and $Pr = 2$.

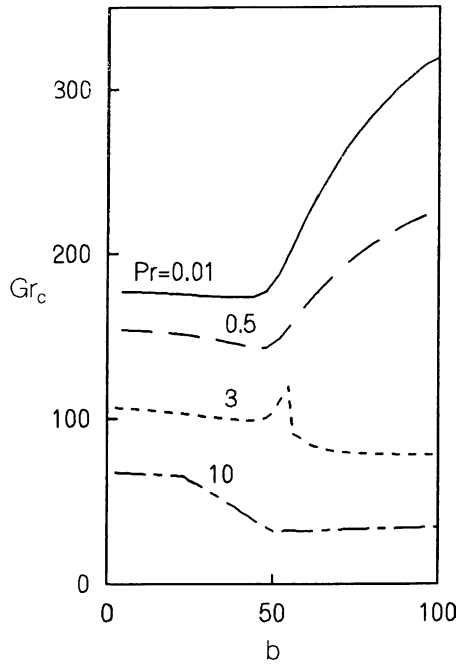

Fig. 9. Gr_c against b for different Pr when $R = 0.1$, $\alpha = 1$ and $C' = 10$.

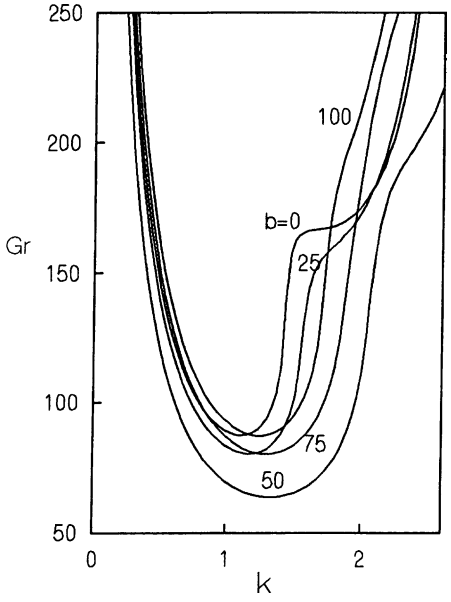

Fig. 8. Marginal stability curves for different b when $R = 0.7$, $\alpha = 1$, $C' = 10$ and $Pr = 2$.

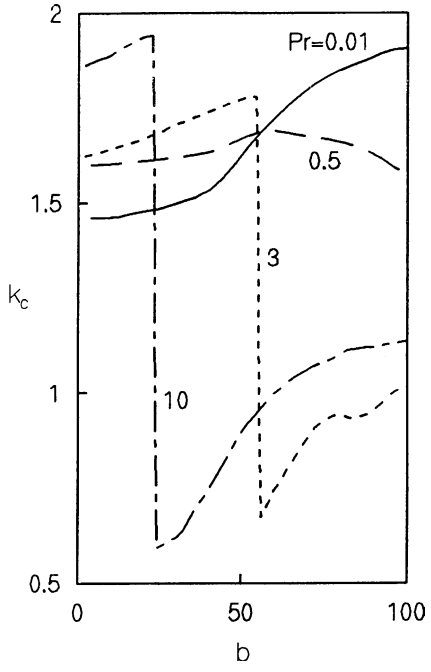

Fig. 10. k_c against b for different Pr when $R = 0.1$, $\alpha = 1$ and $C' = 10$.

The effect of b on the characteristics of the secondary flow at the neutral states, as expressed by the critical wave number k_c and the wave speed c_c are shown in Figs. 10 and 11. The transitions from S to TB mode at $b = 55$ for $Pr = 3$ and $b = 23$ for $Pr = 10$ are marked by jumps in both wave numbers and wave speeds. Physically this means a sudden change in the vertical cell size. This is analogous to those arising in our previous results

[17] where the basic state of convection in a porous annular region was induced by uniformly distributed heat sources. Shaaban and Ozisik [11] obtained a similar jump for negative values of α. The abrupt change in the most dangerous mode at $Pr = 10$ is shown in Fig. 12. We see a sudden reduction in S mode accompanied by the shift of global minimum to TB mode as b increases from 22 to 24. This jump is shifted towards smaller b

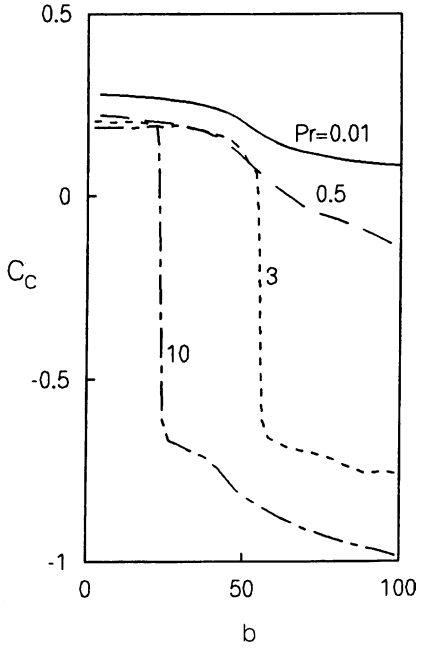

Fig. 11. c_c against b for different Pr when $R = 0.1$, $\alpha = 1$ and $C' = 10$.

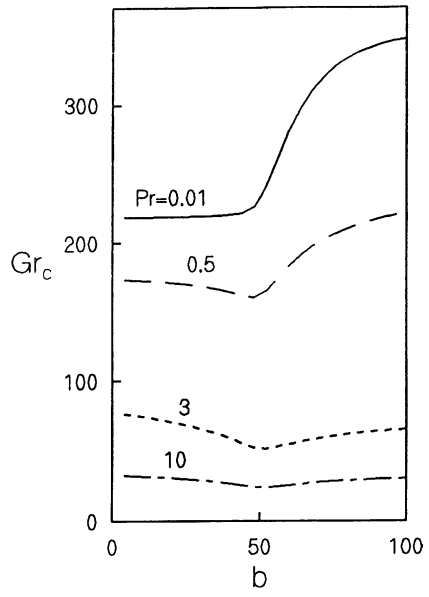

Fig. 13. Gr_c against b for different Pr when $R = 0.4$, $\alpha = 1$ and $C' = 10$.

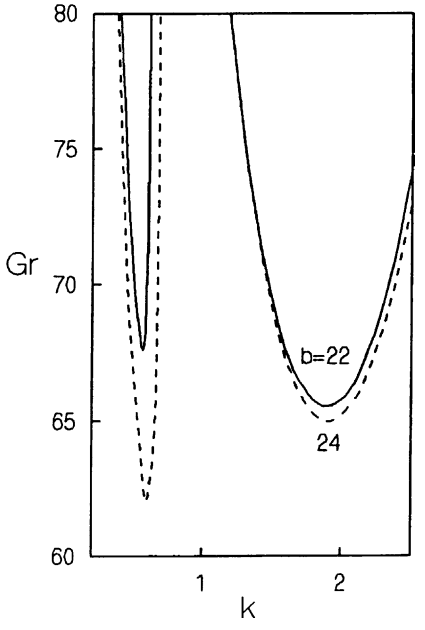

Fig. 12. Change in the critical mode from S to TB.

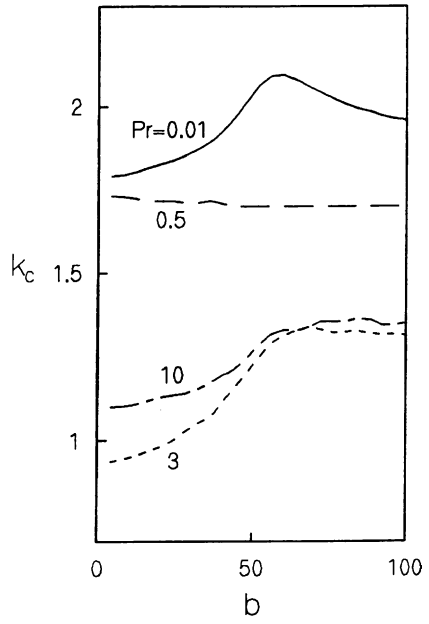

Fig. 14. k_c against b for different Pr when $R = 0.4$, $\alpha = 1$ and $C' = 10$.

for increasing Pr. For the S mode, the wave number is nearly independent of b.

Figs. 13–18 show the stability characteristics for medium ($R = 0.4$) and narrow ($R = 0.7$) gaps respectively. For these gaps, we observe that the basic state at $b = 50$ is always stabilized for moderate and higher values of Pr when b either increases from 50 to 100 or decreases from 50 to 0. More or less symmetrical critical curves about $b = 50$ are seen for $R = 0.7$. The critical wave numbers for $Pr = 0.5$ are nearly unaffected by b for all values of R. This implies that there is not much change in vertical cell size for all gaps when $Pr = 0.5$.

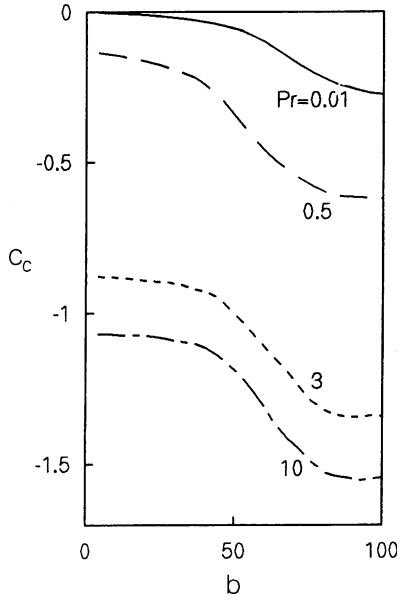

Fig. 15. c_c against b for different Pr when $R = 0.4$, $\alpha = 1$ and $C' = 10$.

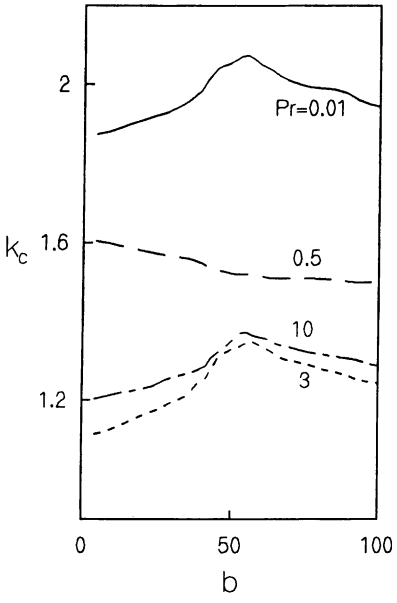

Fig. 17. k_c against b for different Pr when $R = 0.7$, $\alpha = 1$ and $C' = 10$.

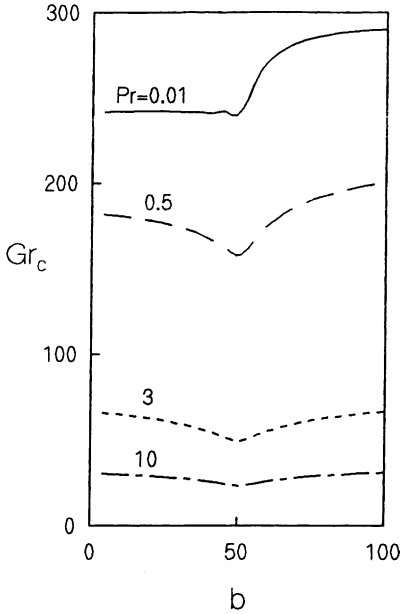

Fig. 16. Gr_c against b for different Pr when $R = 0.7$, $\alpha = 1$ and $C' = 10$.

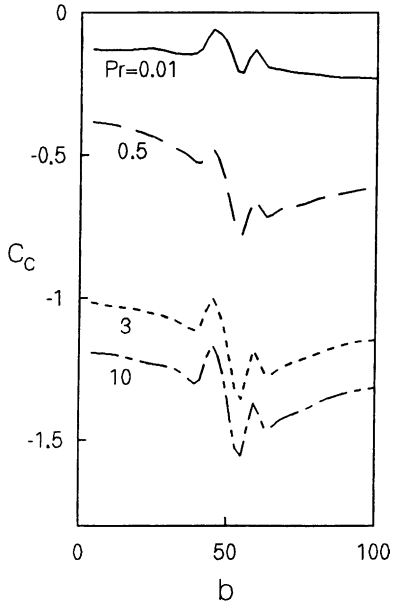

Fig. 18. c_c against b for different Pr when $R = 0.7$, $\alpha = 1$ and $C' = 10$.

No jump as in $R = 0.1$ is observed in the critical wave number and wave speeds for $R = 0.4$ and 0.7. This shows that the effect of R is more on the secondary flow when it takes lower values. A comparison of Figs. 9, 13 and 16 shows that R produces two opposite effects for different Pr. An increase in R stabilizes the flow for $Pr = 0.01$ and 0.5 whereas destabilizes the flow for $Pr = 3$ and 10.

The changes in Gr_c, k_c and c_c against R for different b are plotted in Figs. 19–21 respectively. $R > 0.3$ is always destabilizing. We observe that the maximum points in Gr_c curves are functions of both R and b. A symmetry in the critical stability curves about $b = 50$ is seen as R approaches 0.7 as anticipated. Jumps in k_c from S to TB mode occur when Gr_c reaches a maximum. We find

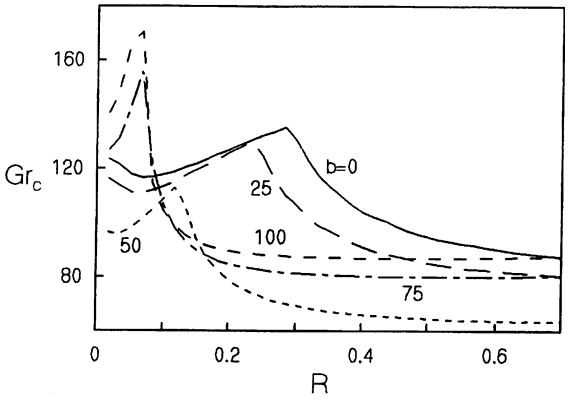

Fig. 19. Gr_c against R for different b when $Pr = 2$, $\alpha = 1$ and $C' = 10$.

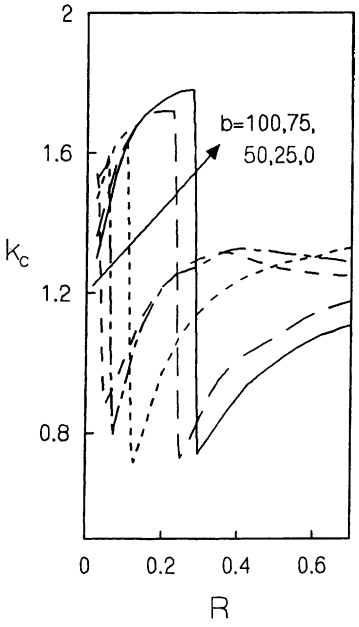

Fig. 20. k_c against R for different b when $Pr = 2$, $\alpha = 1$ and $C' = 10$.

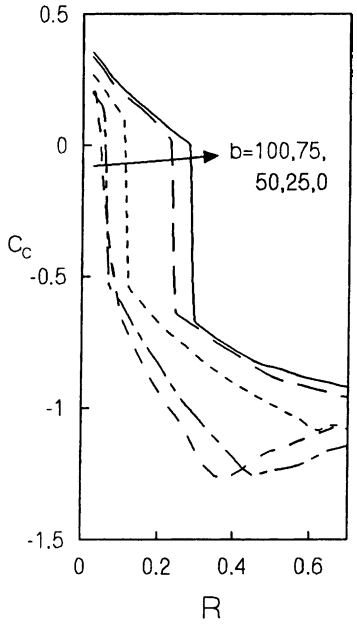

Fig. 21. c_c against R for different b when $Pr = 2$, $\alpha = 1$ and $C' = 10$.

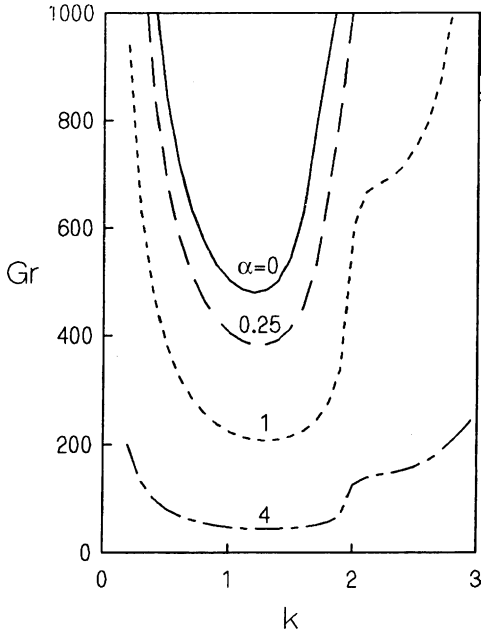

Fig. 22. Marginal stability curves for different α when $R = 0.4$, $Pr = 2$ and $b = 75$.

that these jumps are shifted towards lower R region for increasing b. A peculiar feature is the change in direction of travelling wave perturbations. The upward moving perturbations for low values of R change their direction and start moving downward for higher values of R. An increase in b advances this change.

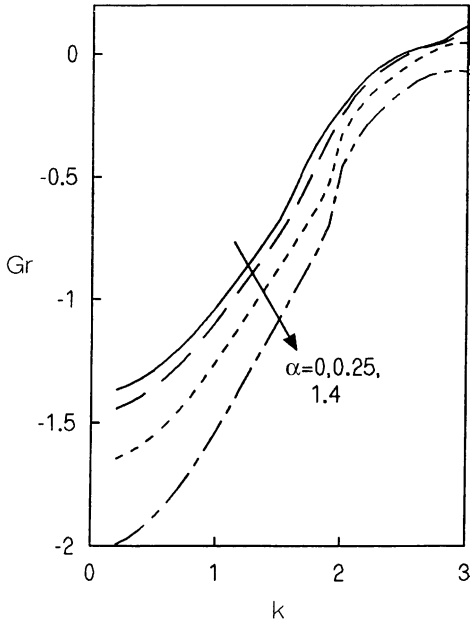

Fig. 23. Marginal wavespeeds for different α when $R = 0.4$, $Pr = 2$ and $b = 75$.

Now let us turn our attention towards the source strength parameter α. Fig. 22 shows that S mode destabilizes convection for increasing α. The corresponding perturbations (Fig. 23) are again travelling waves swept downward and exceed the mainstream velocity as α increases. Fig. 24 displays Gr_c as a function of R and α when $Pr = 2$ and $b = 75$. As we saw earlier Gr_c is found to increase initially and then starts decreasing against R for all values of α. We find that the maximum point of Gr_c is nearly independent of α. The dependence of stability characteristics on α are shown in Figs. 25–27. We notice that the effect of b on Gr_c is almost negligible for larger values of α. But the secondary state represented by k_c and c_c appears to depend much on α.

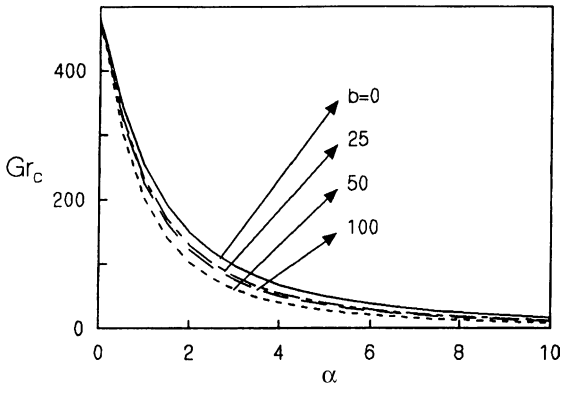

Fig. 25. Gr_c against α for different b when $Pr = 2$ and $R = 0.4$.

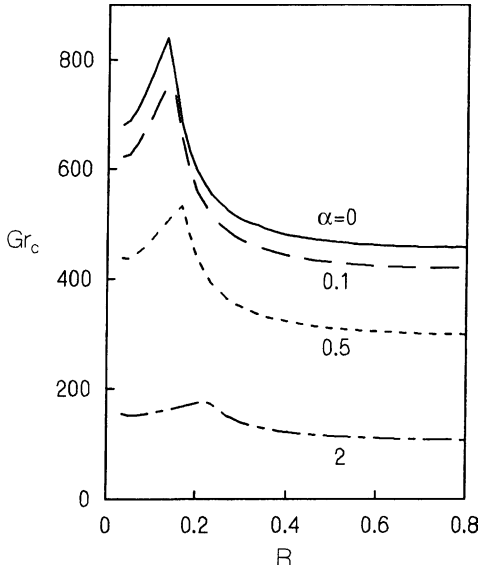

Fig. 24. Gr_c against R for different α, $Pr = 2$ and $b = 75$.

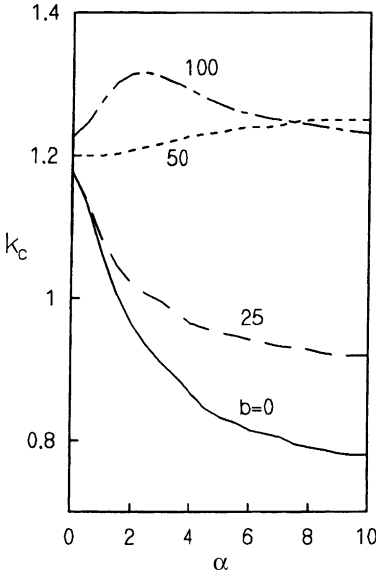

Fig. 26. k_c against α for different b when $Pr = 2$ and $R = 0.4$.

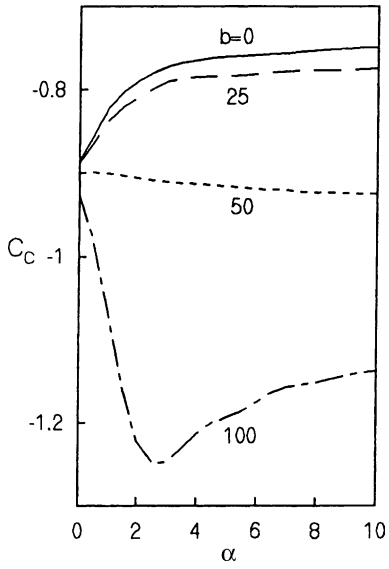

Fig. 27. c_c against α for different b when $Pr = 2$ and $R = 0.4$.

4. Conclusion

The onset of instability of natural convective flow in a fluid contained between two vertical cylinders is greatly dependent on b, α, Pr and R. In general for medium and narrow gaps, the flow remains least stable when $b = 50$. For wider gaps jumps in k_c and c_c are introduced. These jumps are shifted towards the inner cylinder for increasing Pr. Both Pr and α destabilize convection through TB mode of instability. Gr_c plotted against R becomes almost symmetrical about $b = 50$ even when R approaches 0.7. An increase in b shifts the appearance of TB mode towards lower R.

Acknowledgement

This work was done when the first author (S.S) held a Senior Research Fellowship (NET) of CSIR, India.

References

[1] D.A. Vaasquez, Linear stability analysis of convective chemical fronts, Phys. Rev. E 56 (1997) 6767–6773.
[2] M. Garbey, A. Taik, V. Volpert, Influence of natural convection on stability of reaction fronts in liquids, Quart. Appl. Math. LVI (1998) 1–35.
[3] Y.B. Zeldovich, G.I. Barenblatt, V.B. Librovich, G.M. Makhviladze, The Mathematical Theory of Combustion and Explosions, Consultants Bureau, New York, 1985.
[4] E.M. Sparrow, R.J. Goldstein, V.K. Jonsson, Thermal instability in a horizontal layer: Effect of boundary conditions and nonlinear temperature profile, J. Fluid Mech. 18 (1964) 513–528.
[5] S. Acharya, R.J. Goldstein, Natural convection in an externally heated vertical or inclined square box containing internal energy sources, ASME J. Heat Transfer 107 (1985) 855–866.
[6] H.O. May, A numerical study on natural convection in an inclined enclosure containing internal heat sources, Int. J. Heat Mass Transfer 34 (1991) 919–928.
[7] A.G. Churbanov, P.N. Vabishchevich, V.V. Chudanov, V.F. Strizhov, A numerical study on natural convection of a heat generating fluid in rectangular enclosures, Int. J. Heat Mass Transfer 37 (1994) 2969–2984.
[8] A.J. Suo-Antilla, I. Catton, An experimental study of a horizontal layer of fluid with volumetric heating and unequal surface temperatures, AIChE Symposium Series 73 (1976) 72–77.
[9] F.A. Kulacki, R.J. Goldstein, Hydrodynamic instability in fluid layers with uniform volumetric energy sources, Appl. Sci. Res. 31 (1975) 81–109.
[10] A. Yucel, Y. Bayazitoglu, Onset of convection in fluid layers with nonuniform volumetric energy sources, ASME J. Heat Transfer 101 (1979) 666–671.
[11] A.H. Shaaban, M.N. Ozisik, Thermal stability of a vertical fluid layer with volumetric energy source, ASME J. Heat Transfer 107 (1985) 589–595.
[12] A.A. Kolyshkin, R. Vaillancourt, Linear stability of Couette flow with rotating inner cylinder and radially nonuniform internal heat sources, Int. J. Heat Mass Transfer 39 (1996) 537–545.
[13] F. Chen, A.J. Pearlstein, Hot spot locations and temperature distributions in a forced convection photochemical reactor, Int. J. Heat Mass Transfer 36 (1993) 2105–2114.
[14] W.W. Farr, J.F. Gabitto, D. Luss, V. Balakotaiah, Reaction driven convection in a porous medium, AIChE J. 37 (1991) 963–985.
[15] W.B. Gu, C.Y. Wang, Thermal-electrochemical modeling of battery systems, J. Electrochem. Soc. 147 (2000) 2910–2922.
[16] E.J. Davis, R. Zheng, Phoretic force measurement for microparticles under microgravity conditions, in: Proceedings of the Fourth Microgravity Fluids Physics and Transport Phenomena Conference, Cleveland, 1998, pp. 209–214.
[17] S. Saravanan, P. Kandaswamy, Non-Darcian thermal stability of a heat generating fluid in a porous annulus, Int. J. Heat Mass Transfer 46 (2003) 4863–4875.
[18] G.Z. Gershuni, E.M. Zhukhovitskii, A.A. Iakimov, Two kinds of instability of stationary convective motion induced by internal heat sources, Prikl. Mat. Mekh. 37 (1973) 564–568.